Cell

Exosome Transfer from Stromal to Breast Cancer Cells Regulates Therapy Resistance Pathways

Mirjam C. Boelens,[1,3,8,9] Tony J. Wu,[1,3,8] Barzin Y. Nabet,[1,3,8] Bihui Xu,[1,3] Yu Qiu,[1,3] Taewon Yoon,[1,3] Diana J. Azzam,[5] Christina Twyman-Saint Victor,[2,3] Brianne Z. Wiemann,[1] Hemant Ishwaran,[4] Petra J. ter Brugge,[7] Jos Jonkers,[7] Joyce Slingerland,[5,6] and Andy J. Minn[1,3,*]

[1]Department of Radiation Oncology

[2]Department of Medicine, Division of Gastroenterology

[3]Abramson Family Cancer Research Institute

Perelman School of Medicine, University of Pennsylvania, Philadelphia, PA 19104, USA

[4]Department of Public Health Sciences, Division of Biostatistics

[5]Department of Biochemistry & Molecular Biology, Braman Family Breast Cancer Institute at Sylvester, Sylvester Comprehensive Cancer Center

[6]Department of Medicine

Miller School of Medicine, University of Miami, Miami, FL 33136, USA

[7]Division of Molecular Pathology, Netherlands Cancer Institute, Plesmanlaan 121, 1066 CX Amsterdam, the Netherlands

[8]Co-first author

[9]Present address: Netherlands Cancer Institute, Division of Molecular Pathology, Plesmanlaan 121, 1066 CX Amsterdam, the Netherlands

*Correspondence: andyminn@exchange.upenn.edu

http://dx.doi.org/10.1016/j.cell.2014.09.051

SUMMARY

Stromal communication with cancer cells can influence treatment response. We show that stromal and breast cancer (BrCa) cells utilize paracrine and juxtacrine signaling to drive chemotherapy and radiation resistance. Upon heterotypic interaction, exosomes are transferred from stromal to BrCa cells. RNA within exosomes, which are largely noncoding transcripts and transposable elements, stimulates the pattern recognition receptor RIG-I to activate STAT1-dependent antiviral signaling. In parallel, stromal cells also activate NOTCH3 on BrCa cells. The paracrine antiviral and juxtacrine NOTCH3 pathways converge as STAT1 facilitates transcriptional responses to NOTCH3 and expands therapy-resistant tumor-initiating cells. Primary human and/or mouse BrCa analysis support the role of antiviral/NOTCH3 pathways in NOTCH signaling and stroma-mediated resistance, which is abrogated by combination therapy with gamma secretase inhibitors. Thus, stromal cells orchestrate an intricate crosstalk with BrCa cells by utilizing exosomes to instigate antiviral signaling. This expands BrCa subpopulations adept at resisting therapy and reinitiating tumor growth.

INTRODUCTION

The elucidation of resistance mechanisms to chemotherapy and radiation is an important goal in improving cancer survival. Previously, we characterized a gene signature for radiation (RT) and chemotherapy (chemo) resistance that was discovered through in vivo selection for RT-resistant tumors (Khodarev et al., 2004; Weichselbaum et al., 2008). Because the majority of the genes identified were interferon-stimulated genes (ISGs), which normally are activated as part of an antiviral response, we termed this signature the interferon-related DNA damage resistance signature (IRDS). Several IRDS genes, including the transcription factor *STAT1*, influence RT/chemo resistance in cell lines and mouse tumor models. Interrogation across the most common human cancers revealed that a large proportion of untreated primary tumors express the IRDS. In breast cancer, IRDS expression measured by a clinical classifier comprised of seven IRDS genes (*STAT1*, *MX1*, *ISG15*, *OAS1*, *IFIT1*, *IFIT3*, and *IFI44*) identifies patients whose cancers are resistant to chemo and RT. Thus, the IRDS may represent a common and inherent mechanism of resistance across various human cancers. How the IRDS is regulated and how ISGs can protect against RT/chemo is unclear.

A common way that ISGs are activated is through pattern recognition receptors (PRRs) that are triggered by pathogen-associated molecular patterns such as viral nucleic acids (Loo and Gale, 2011). PRRs include toll-like receptors (TLRs) and RIG-I-like receptors. Typically, RIG-I is activated by 5′-triphosphate viral RNA after viruses gain entry into immune and non-immune cells. However, PRRs can also be activated through alternative routes by exosomes, which are small membrane vesicles capable of transferring contents between cells to function in cell-cell communication (Théry et al., 2009). Exosomes can transfer viral RNA from infected cells to trigger an interferon response in immune cells, presumably through TLRs, to enhance viral suppression (Dreux et al., 2012; Li et al., 2013b). In cancer,

exosomes secreted by tumor cells can increase metastasis through interaction with cells of the microenvironment (Fabbri et al., 2012; Peinado et al., 2012). Alternatively, exosomes from mesenchymal cells can be transferred to cancer to promote metastasis (Luga et al., 2012). Thus, these recent data suggest that PRRs and exosomes orchestrate heterotypic cell-cell communication to regulate antiviral responses or to aid cancer progression. Whether crosstalk between cancer and the tumor microenvironment can use exosomes and PRRs to similarly control ISG/IRDS expression or influence treatment resistance is unknown.

The importance of the tumor microenvironment in dictating treatment response is increasingly evident. Stromal cells, which are primarily fibroblasts but can also be other cell types, can promote survival after genotoxic and targeted therapy through the secretion of paracrine factors (McMillin et al., 2013). Many of these interactions between stromal cells and tumor cells may support the maintenance of cancer stem-like cells (i.e., tumor-initiating cells) analogously to how normal stem cells depend on a niche (Korkaya et al., 2011). Because tumor-initiating cells are resistant to RT/chemo and their survival would allow efficient tumor regrowth, understanding how the stromal microenvironment can influence these therapy resistant cells may provide promising new drug targets.

The NOTCH family of receptors activates developmental signaling pathways that have multiple roles in cancer, including drug resistance (McAuliffe et al., 2012; Ranganathan et al., 2011) and the regulation of tumor-initiating cells (Azzam et al., 2013). Activation requires cell-cell contact and engagement of NOTCH ligands, such as JAGGED proteins. Given the properties of the NOTCH pathway in cancer, there is a significant interest in targeting the pathway as a cancer therapeutic. Activation of NOTCH occurs through the cleavage of its intracellular domain and can be blocked by a gamma secretase inhibitor (GSI). Currently, there are multiple clinical trials testing GSIs combined with other targeted agents and conventional chemotherapy (Aster and Blacklow, 2012). However, challenges exist that include lack of a companion biomarker to identify patients who will benefit from NOTCH inhibition. Understanding how NOTCH can be activated in subsets of cancers may facilitate their utilization as drug targets.

In this study, we integrate experimental and computational models to investigate how stromal cells communicate with breast cancer to regulate expression of ISGs. In so doing, we define an antiviral pathway that is activated by exosomes and RIG-I and cooperates with NOTCH3 to regulate stroma-mediated expansion of therapy-resistant cells.

RESULTS

Stromal Cells Induce the IRDS and Increase Breast Cancer Radiation Resistance

Previous reports indicate that ISGs can be modulated by the microenvironment (Buess et al., 2007). To examine whether the microenvironment can influence IRDS expression and contribute to RT/chemo resistance, we utilized metastatic MDA-MB-231 breast cancer cells (1833) (Kang et al., 2003) expressing a GFP-luciferase reporter and xenografted them with or without nontransformed MRC5 human diploid fibroblasts used as stromal cells. Tumors containing admixed fibroblasts exhibited high expression of several IRDS genes, including *STAT1* (Figure 1A), particularly from breast cancer cells (Figure 1B). In contrast, tumors arising from breast cancer cells alone had lower STAT1/ISG expression and remained primarily comprised of human breast cancer cells, suggesting poor stromalization by mouse cells. The presence of admixed fibroblasts enhanced the growth rate of breast cancer cells (Figure 1C), which is a defining property of carcinoma-associated fibroblasts (CAFs), as measured by the rate of change in bioluminescence signal at each time point. After RT, breast cancer cells from tumors without admixed fibroblasts promptly stopped growing and showed regression by day 24. In contrast, breast cancer admixed with fibroblasts showed dramatically reduced cell death (Figure 1D) and maintained significant growth even after RT (Figure 1C). In total, these observations suggest a relationship between tumor and stromal cell interaction, antiviral signaling, and survival of cells adept at resisting DNA damage and sustaining tumor growth.

Stroma-Mediated IRDS Induction and Protection Are STAT1 Dependent and Specific for Basal-like Breast Cancers

To better examine the relationship between IRDS expression and stroma-mediated protection across different breast cancer and stromal cell combinations, we cocultured both cell types in vitro to model stroma-mediated resistance (referred to as coculture) and discovered that breast cancer cells can be divided into two groups. The first group, called ''IRDS responders'' (IRDS-Rs), is enriched in the basal-like subtype (Table S1 available online) and upregulated IRDS genes after interaction with MRC5 fibroblasts (Figure 1E). The second group, called ''IRDS nonresponders'' (IRDS-NRs), is composed of non-basal-like and some basal-like subtypes and failed to induce IRDS genes. Importantly, only IRDS-Rs were protected by fibroblasts after RT (Figure 1F) or after chemotherapy (Figure 1G). Multiple other stromal cell lines (CAFs, bone marrow, and fibroblasts) able to induce the IRDS were also able to promote resistance against RT (Figure S1A); however, not all stromal cells were protective, as illustrated by a macrophage cell line that neither induced the IRDS nor protected (Figure S1B). Genome-wide transcriptomic analysis from coculture of IRDS-R compared to monoculture (Table S1) demonstrated upregulation of nearly all IRDS genes in breast cancer (Figures 1H and S1C and Table S2). Stroma-mediated induction of IRDS was specific to IRDS-R breast cancer (Table S3). Knockdown of STAT1 in 1833 IRDS-R prior to coculture with MRC5 fibroblasts depressed nearly all IRDS genes compared to control (Figure 1H) and also inhibited stroma-mediated resistance (Figure 1I), a result observed with multiple different siRNAs targeting STAT1 (Figures S1D and S1E). Stable STAT1 knockdown (Figures S1D and S1E) also selectively inhibited the protective effects of MRC5 fibroblasts as measured by an in vitro luciferase-based assay (Figure 1J). In the absence of RT, disruption of STAT1 had negligible effects on growth with or without fibroblasts (Figure S1F). Thus, a subset of basal subtype breast cancers can interact with multiple stromal cell types to increase IRDS genes and RT/chemo resistance in a STAT1-dependent manner.

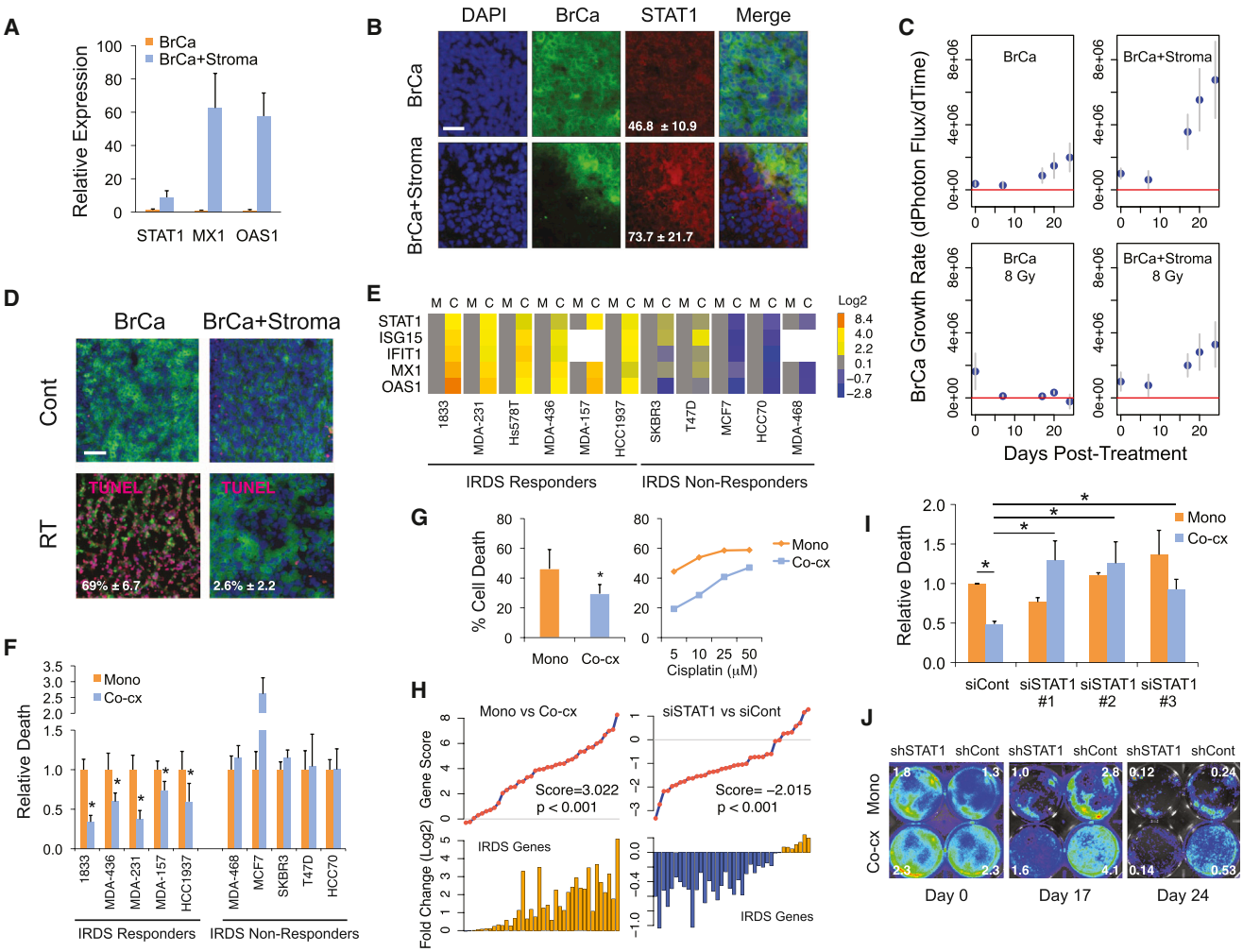

Figure 1. Stromal Cells Induce ISGs and Protect Basal-like Breast Cancer Cells against Radiation in a STAT1-Dependent Manner

(A) Human MDA-MB-231 metastatic breast cancer cell (BrCa) line (1833) was admixed with or without MRC5 normal human fibroblasts (stroma), and expression of IRDS genes was determined by qRT-PCR.

(B) GFP-labeled 1833 breast cancer cells with and without MRC5 fibroblasts were xenografted subcutaneously into nude mice, and tumors were imaged (20×) at day 14. STAT1 intensity in breast cancer cells is quantitated for representative field shown. Scale bar, 100 microns.

(C) Bioluminescence imaging (BLI) response of 1833 breast cancer cells with a luciferase reporter gene after xenografting with and without MRC5 fibroblasts. Tumors were irradiated with 8 Gy (day 0). Shown is change in photon flux over time (first derivative, mean ± SEM, n = 5–10). Positive first derivative indicates growth, zero indicates no growth, and negative values denote regression. Data are a separate analysis of the control groups from Figure 5M.

(D) 1833 breast cancer cells were stained with GFP and TUNEL (red) 10 days after RT. Percent TUNEL positive is shown. Scale bar, 100 microns.

(E) Breast cancer cells (Table S1) were classified as IRDS responders (IRDS-Rs) or IRDS nonresponders (IRDS-NRs). Heat map and scale show breast cancer IRDS genes after monoculture (M) or MRC5 coculture (C).

(F) Cell death of IRDS-Rs and IRDS-NRs 4 days after 10 Gy RT in mono- (Mono) and coculture (Co-cx) (n = 3–10).

(G) Cell death of 1833 IRDS-R after cisplatin chemotherapy (n = 3) and after dose response.

(H) Gene Set Analysis shows changes in IRDS genes 48 hr after coculture versus monoculture of IRDS-Rs (left; also see Table S1) or after STAT1 knockdown in 1833 IRDS-R in coculture (right). Top graph plots individual and overall gene scores, and bottom graph shows fold change.

(I) Cell death of 1833 IRDS-R 4 days after 10 Gy RT using three independent siRNAs to STAT1.

(J) BLI-based survival assay after 10 Gy RT (day 0) using luciferase-labeled 1833 cells with shSTAT1 or control knockdown (shCont). Photon flux ($\times 10^6$) for each well is indicated. Shown is representative experiment (n = 5). *p < 0.05.

Unless noted, all bar plots in figure are mean ± SD of *n* biological replicates. See also Figure S1.

IRDS Induction Is Controlled by RIG-I

Stroma-mediated IRDS induction and resistance requires live stromal cells and does not associate with expression and/or function of interferons or interferon receptors (Figures S2A–S2E). To explore alternative pathways to IRDS induction, we examined the transcriptome of IRDS-R breast cancer cells in MRC5 coculture compared to monoculture. Among the upregulated genes (Table S2) were several PRRs known to activate

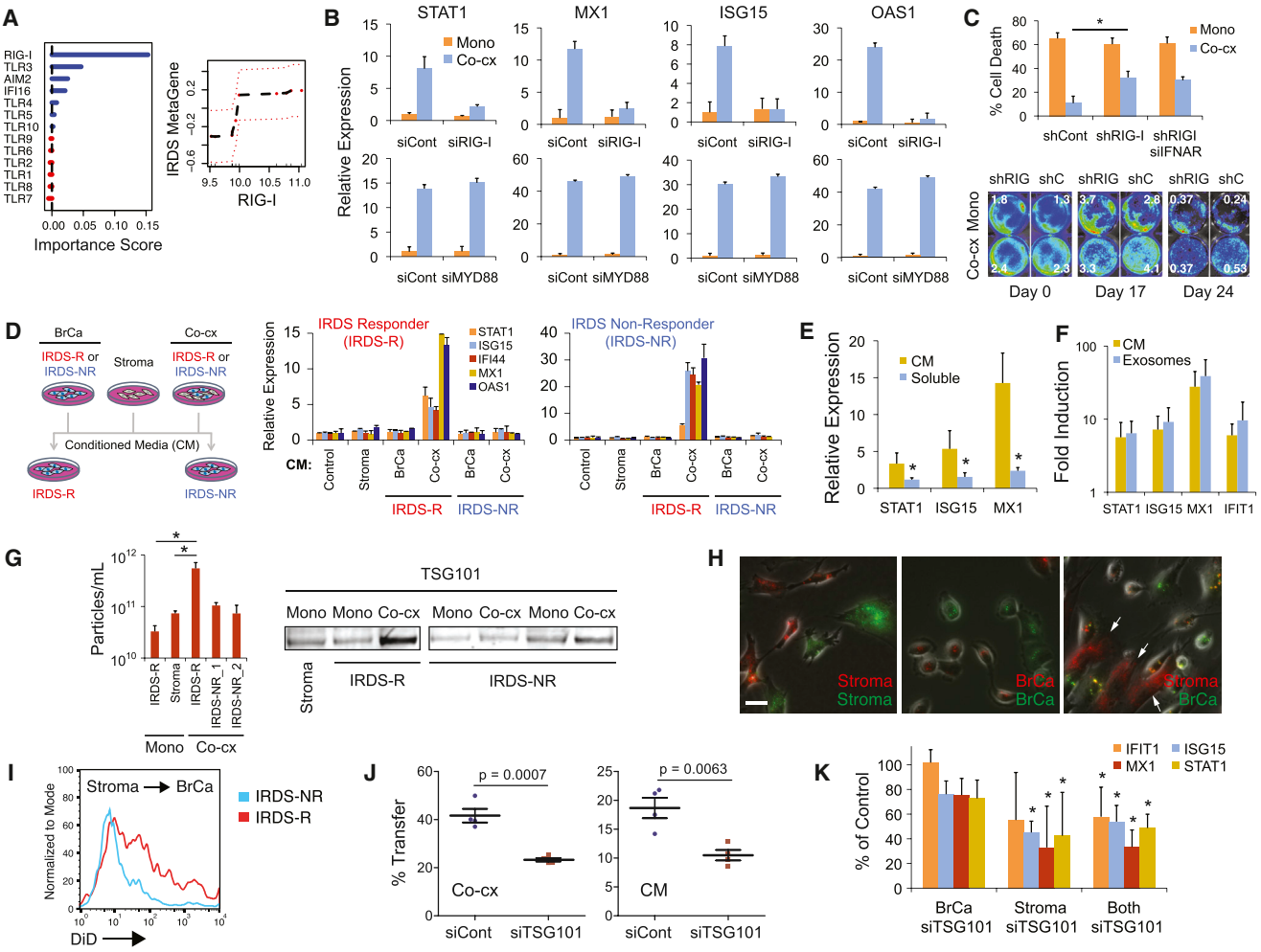

Figure 2. Stromal Cell Interaction Increases Exosomes that Upregulate ISGs through a RIG-I Antiviral Pathway

(A) Importance scores (higher is more predictive) of PRRs from a multivariable RF regression model to predict induction of IRDS after MRC5 coculture with IRDS-Rs. The model explains 60.8% of the total variance. Adjusted effect of *RIG-I* on IRDS metagene expression is shown on right (red dashes are ± 2 SE).

(B) Expression of IRDS genes after siRNA to RIG-I (top row) or MYD88 (bottom row) in 1833 IRDS-R. Shown is a representative experiment (n = 3).

(C) Cell death of 1833 IRDS-R after RT (n = 4) and a representative BLI-based survival assay (n = 2) after the indicated knockdown (RT on day 0). Photon flux ($\times 10^6$) for each well is shown. The control is same as Figure 1J.

(D) Expression of IRDS genes in 1833 IRDS-R (middle) or MCF7 IRDS-NR (right) after addition of conditioned media (CM) from MRC5 fibroblasts (Stroma), IRDS-R or IRDS-NR (BrCa), or MRC5 coculture with IRDS-Rs or IRDS-NRs (co-cx). See schematic (left).

(E) CM collected after 48 hr or the soluble fraction from CM (soluble) was applied to 1833 IRDS-R, and expression of IRDS genes was examined (n = 4).

(F) Fold induction of IRDS genes in 1833 IRDS-R after addition of coculture CM or purified exosomes (n = 5).

(G) NanoSight quantification of exosomes (left) from 1833 IRDS-R, MRC5 fibroblasts (Stroma), and MRC5 coculture using either 1833 IRDS-R or IRDS-NR (MDA-MB-468, IRDS-NR_1; MCF7, IRDS-NR_2). Immunoblot for TSG101 (right) using 1833 IRDS-R or IRDS-NR (MDA-MB-468, lanes 4–5; MCF7, lanes 6–7).

(H) MRC5 fibroblasts (stroma) or 1833 IRDS-R were labeled with green or red lipophilic dye in monoculture (left and middle). For coculture (right), MRC5 (arrows) were labeled red, and breast cancer cells were labeled green. Scale bar, 40 microns.

(I) Representative flow cytometry of DiD dye transfer from MRC5 stroma to 1833 IRDS-R or MDA-MB-468 IRDS-NR.

(J) Exosome transfer from coculture after TSG101 knockdown (left) and after addition of the coculture CM cleared of debris and apoptotic bodies (right) (n = 4).

(K) IRDS gene induction by coculture CM after TSG101 knockdown in 1833 IRDS-R, MRC5 stroma, or both (n = 3). Gene expression and significance levels are relative to siControl. *p < 0.05.

Unless noted, all bar plots in figure are mean ± SD of *n* biological replicates. See also Figure S2.

ISGs. Random forest (RF) multivariable regression analysis (Chen and Ishwaran, 2012) of these and other similar PRRs demonstrated that increasing expression of RIG-I best explains the upregulation of IRDS genes by fibroblasts (Figure 2A). Accordingly, knockdown of RIG-I in 1833 IRDS-R inhibited IRDS gene induction after coculture, whereas disruption of MYD88, which is required for signaling by multiple TLRs not predicted to regulate the IRDS, had no effect (Figures 2B and S2F). Disruption of RIG-I by shRNA (Figure S2F) also partially reversed stroma-mediated resistance, as measured by short- and

long-term survival (Figure 2C), without influencing general cell proliferation (Figure S2G). Concomitant disruption of the type one interferon receptor with RIG-I had no additive effect. Thus, STAT1/IRDS induction and stromal protection are primarily initiated through RIG-I rather than interferon receptors.

Exosomes Are Transferred from Stromal Cells to Breast Cancer to Increase IRDS

Conditioned media (CM) from coculture of IRDS-Rs with stromal fibroblasts, but not from stromal coculture of IRDS-NRs or from monoculture, upregulate IRDS genes when applied to monocultured IRDS-Rs (Figure 2D). Interestingly, CM from coculture of IRDS-Rs also upregulates IRDS when applied to IRDS-NRs. These results suggest that stromal cell interaction with IRDS-Rs produces a secreted factor capable of activating RIG-I. Recent evidence suggests that some PRRs can be activated by exosomes. Consistent with a role for exosomes in IRDS activation, the exosome-depleted soluble fraction of CM poorly induced the IRDS (Figure 2E). Conversely, addition of purified exosomes, which were confirmed by electron microscopy and by analyses of size properties and markers (Figure S2H), was sufficient to induce IRDS genes (Figure 2F).

To examine how coculture with IRDS-Rs influences exosome secretion and possible transfer to breast cancer cells, exosomes were quantified by particle counting and by the exosome marker TSG101. Both methods indicated that more exosomes were present after coculture of IRDS-Rs compared to either IRDS-NRs or monoculture (Figure 2G). To examine exosome transfer, stromal cells and/or breast cancer cells were differentially labeled with either red or green fluorescent lipophilic dye to mark exosomes. For both cell types, dye transfer in monoculture appeared minimal (Figure 2H). In coculture, microscopy and flow cytometry revealed an apparent unidirectional transfer of exosomes from fibroblasts preferentially to IRDS-Rs, but not to IRDS-NRs (Figures 2H, 2I, S2I, and S2J). Multiple stromal cell types capable of inducing the IRDS were also able to transfer exosomes to IRDS-Rs (Figure S2K). Transfer was also observed upon addition of coculture CM cleared of debris and apoptotic bodies (Figure 2J). With both assays, transfer was mitigated by knockdown of TSG101 (Figures 2J and S3C), which is a regulator of exosome biogenesis. Accordingly, TSG101 disruption in fibroblasts, but not in breast cancer cells, also inhibited IRDS induction without affecting elevation in non-IRDS genes such as *MMP1* and *CXCL1* (Figures 2K and S3D). Thus, IRDS-Rs, but not IRDS-NRs, coerce an increase in secretion of exosomes by stromal cells that results in transfer to breast cancer cells and subsequent IRDS induction.

Exosome Transfer Is Regulated by Stromal RAB27B

To determine whether the increased production of exosomes in coculture primarily originated from stromal or breast cancer cells, we used a protein array of well-known exosome markers. This revealed that coculture exosomes were much more similar to exosomes from fibroblasts compared to those from breast cancer cells (Figure 3A), arguing that enhanced exosome production in coculture is primarily from stromal cells. Interrogation of stromal RAB GTPases commonly implicated in exosome secretion (Raposo and Stoorvogel, 2013) revealed that stromal RAB27B transcript and protein were consistently induced after fibroblasts were cocultured with IRDS-Rs, but not with IRDS-NRs (Figures 3B and S3A). Indeed, of all RAB GTPases on the microarray, RAB27B was elevated the most in fibroblasts after interaction specifically with IRDS-Rs (Figure S3B). Knockdown of RAB27B in fibroblasts (Figure S3C) inhibited the ability of CM from coculture to stimulate IRDS genes (Figure 3C) but had no effect on non-IRDS genes such as *MMP1* and *CXCL1* (Figure S3D). Accordingly, knockdown of RAB27B also interfered with exosome transfer from fibroblasts to IRDS-Rs (Figure 3D), a result observed with multiple siRNAs to RAB27B (Figure S3E). In contrast, inhibition of RAB27A, which was not differentially expressed in fibroblasts, had no effect (Figure S3F). In total, these data argue that exosome transfer from stromal to breast cancer cells and subsequent IRDS induction is regulated by stromal RAB27B.

5′-Triphosphate Exosome RNA Activates RIG-I to Induce the IRDS

Because exosomes and RIG-I both influence the effects of stromal cells, we focused on a potential relationship between the two. When RIG-I was disrupted in 1833 IRDS-R, IRDS gene induction by coculture CM and by purified exosomes was similarly inhibited (Figures 3E and 3F). RIG-I activation typically results from binding to viral RNA through recognition of specific motifs such as 5′-triphosphates rather than through sequence specificity (Loo and Gale, 2011). To investigate whether exosome RNA (exoRNA) can induce IRDS through RIG-I, exoRNA from coculture exosomes was re-encapsulated into synthetic lipid vesicles and transfected into monoculture 1833 IRDS-R. Whereas total cellular RNA from coculture failed to induce IRDS genes, exoRNA upregulated IRDS genes in a RIG-I-dependent manner to levels that were comparable to a viral HCV RNA used as a positive control (Figure 3G). In contrast, HCV RNA or exoRNA did not significantly increase non-IRDS genes such as *IFI16*, which normally responds to cytosolic DNA. Treatment with RNase, but not DNase, eliminated the ability of exoRNA, as well as an in-vitro-transcribed 5′-triphosphate control RNA (IVT5′ppp), to elevate IRDS genes (Figure 3H). Removal of 5′-phosphates revealed that the active RNA contains exposed 5′-phosphate ends and is not a typical protein-coding mRNA with a 5′-cap (Figure 3I). Consistent with the known specificity of RIG-I for 5′-triphosphate, IRDS induction was inhibited after specific removal of 5′-triphosphate from exoRNA or from the IVT5′ppp, whereas digestion of RNA containing 5′-monophosphate had no effect. Thus, exoRNA containing 5′-triphosphate activates RIG-I to induce IRDS genes.

Sequencing of exoRNA isolated from coculture of 1833 IRDS-R revealed no apparent match to viral genomes from 19 different viruses known to activate RIG-I. Instead, enrichment for human intergenic and noncoding transcripts was observed in exoRNA compared to total cellular RNA from coculture (Figure 3J). In both cellular RNA and exoRNA, repetitive sequences accounted for a significant fraction of these intergenic transcripts; however, although snRNA-like repeats were the predominant class of repetitive elements in cellular RNA, transposable elements represented the largest class within exoRNA. Specifically, SINEs, LINEs, and long terminal repeat (LTR) retrotransposons were

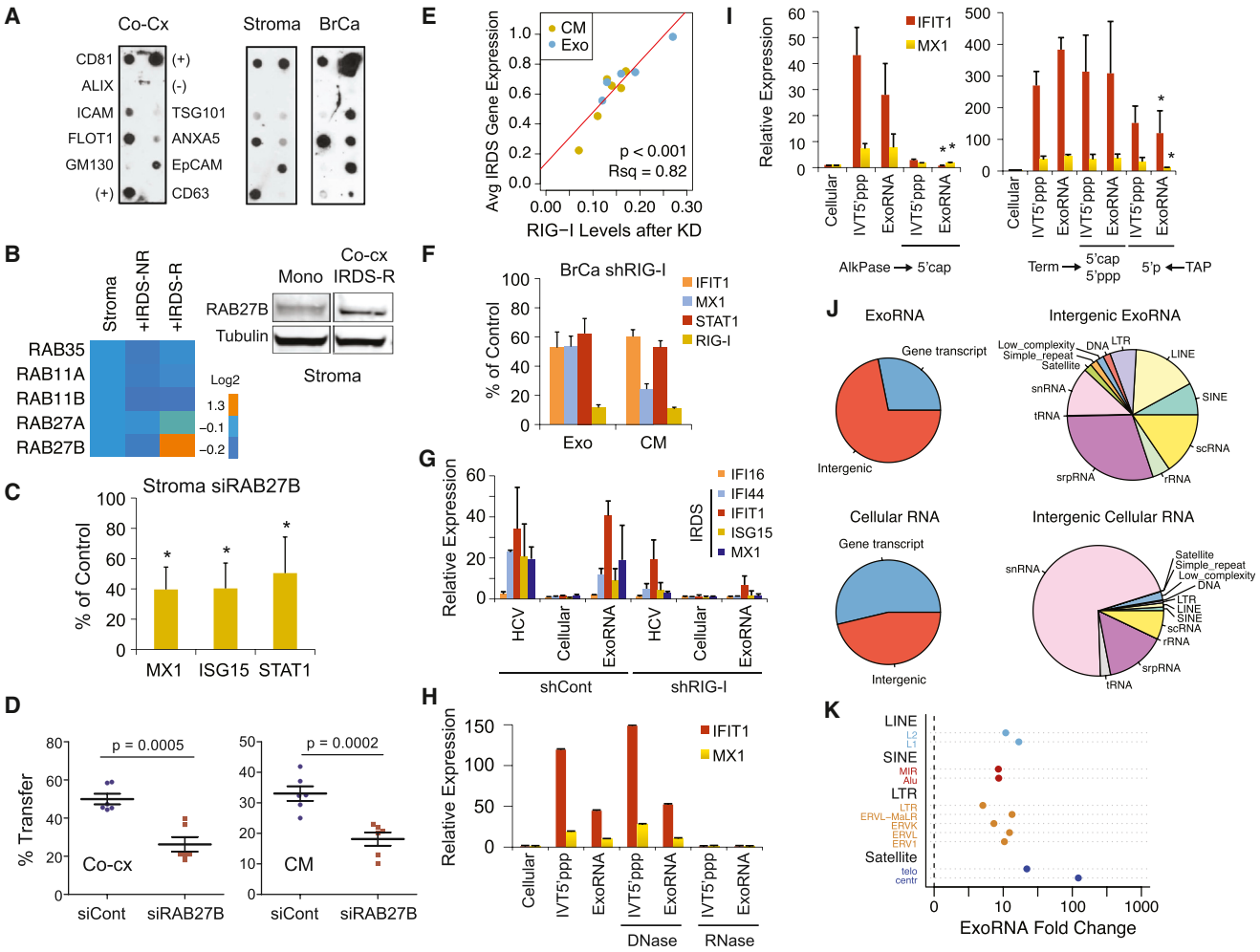

Figure 3. Stromal Exosomes Are Regulated by RAB27B and Transfer 5′-Triphosphate RNA to Activate RIG-I in Breast Cancer Cells

(A) Exosomes were isolated from monoculture of MRC5 fibroblasts (Stroma) or 1833 IRDS-R (right) or from coculture (left) and profiled by antibody array for the indicated exosome markers. GM130 is a check for cellular contamination. Positive (+) and negative (−) controls are labeled.

(B) Averaged microarray expression of the indicated RABs from MRC5 in monoculture (stroma) or after coculture with IRDS-R or IRDS-NR are shown as a heat map. Immunoblot (right) for RAB27B protein expression in MRC5 after coculture with MDA-MB-157 or 1833 IRDS-R (Figure S3A) compared to MRC5 monoculture.

(C) IRDS expression in 1833 IRDS-R after addition of CM isolated from coculture using MRC5 transfected with siRAB27B compared to siControl (n = 3).

(D) Exosome transfer to 1833 IRDS-R after coculture with or without RAB27B knockdown (left) or addition of coculture CM cleared of debris and apoptotic bodies (right).

(E) Average IRDS gene expression (mean expression of *IFIT1*, *MX1*, and *STAT1*) in response to exosomes (Exo, n = 5) or coculture CM (n = 6) plotted against *RIG-I* levels after knockdown in 1833 IRDS-R.

(F) IRDS gene expression from two representative data points used to generate plot in Figure 3E are shown relative to siControl.

(G) IRDS gene expression after RNA from exosomes (ExoRNA), cellular RNA, or a positive control HCV RNA was transfected into 1833 IRDS-R with or without RIG-I knockdown (n = 4). *IFI16* is a non-IRDS gene used as a negative control.

(H and I) (H) Expression of IRDS genes *IFIT1* and *MX1* resulting from transfection of ExoRNA after RNase treatment or (I) removal of 5′-monophosphate (5′-p) and/or 5′-triphosphate (5′-ppp) (n = 3). An in-vitro-transcribed 5′-ppp RNA (IVT5′ppp) is used as a positive control. Shown are RNA motifs remaining after enzyme modification with alkaline phosphatase (AlkPase), Terminator exonuclease (Term), and tobacco acid pyrophosphatase (TAP). IVT5′ppp serves as a control for RNA enzyme modification by AlkPase and TAP.

(J) Distribution of known gene transcripts and intergenic transcripts from rRNA-depleted exoRNA and cellular RNA from 1833 IRDS-R coculture (left). Distribution of major repetitive elements and transposable element classes for intergenic transcripts are shown on right.

(K) ExoRNA enrichment for major subfamilies of transposable elements and satellite sequences compared to cellular RNA. *p < 0.05.

Unless noted, all bar plots in figure are mean ± SD of *n* biological replicates. See also Figure S3.

markedly enriched among exoRNA repetitive elements, with the most prevalent subclasses augmented by 10-fold or more (Figure 3K). Other repetitive sequences such as telomeric and centromeric satellite sequences were present at lower frequencies but demonstrated 100- to 1,000-fold enrichment in exoRNA. Because transposable elements are one category of

RNA polymerase III transcripts, which can have 5′-triphosphate ends (Belancio et al., 2010; Dieci et al., 2013), their enrichment suggests that they may contribute to exoRNAs capable of stimulating RIG-I.

Stroma-Mediated Paracrine Antiviral Signaling and Juxtracrine NOTCH3 Signaling Enhance Transcription of NOTCH Target Genes

Although RIG-I and STAT1 are necessary for stroma-mediated resistance, separation of breast cancer cells from stromal fibroblasts using a transwell filter large enough for exosome passage resulted in retained IRDS induction but loss of RT resistance (Figure 4A). This suggests that the antiviral pathway may work with an additional juxtacrine pathway to control stroma-mediated protection. To explore this, we computationally constructed a juxtacrine interactome between IRDS-Rs and fibroblasts using differentially expressed genes from each cell type combined with protein-protein interaction data (Figure S4A). This revealed that NOTCH3 expression was increased in IRDS-R breast cancer cells after coculture, and its membrane-bound ligand JAG1 was both induced in fibroblasts and constitutively elevated in IRDS-Rs. Protein analysis confirmed that NOTCH3 was expressed at low levels in 1833 IRDS-R, but both its expression and its cleaved intracellular domain increased after fibroblast interaction (Figure 4B). In contrast, expression of NOTCH1, 2, and 4 did not change.

To investigate how antiviral signaling and NOTCH3 might interact, we explored whether STAT1 facilitates transcription of NOTCH-dependent genes. Gene set enrichment analysis of NOTCH target genes, which we defined by GSI washout experiments (Table S4), confirmed upregulation of NOTCH targets in IRDS-Rs, but not IRDS-NRs after coculture (Figure 4C). Knockdown of STAT1 not only inhibited stroma-mediated upregulation of NOTCH target mRNAs (Figure 4D) but also blunted the primary transcripts for canonical NOTCH targets *HES1* and *HEY1* (Figure 4E), which is consistent with STAT1 exerting transcriptional control over these genes. To better characterize this, we utilized doxycycline inducible NOTCH3 intracellular domain (NICD3) to constitutively activate NOTCH3 in 1833 IRDS-R and added exosome-containing CM to initiate antiviral signaling. As measured by the *HEY1* primary transcript, CM augmented responsiveness to NICD3 (Figure 4F). Depletion of exosomes from CM inhibited this effect on the *HEY1* primary transcript (Figure 4G) and mRNA (Figure S4B), and similar results were noted for *HES1*. The exosome-dependent increase in *HEY1* and *HES1* transcripts in the absence of NICD3 induction is likely due to baseline NOTCH and/or leakiness of the inducible system.

Interrogation of ENCODE data revealed STAT1 occupancy at several locations within active proximal promoters of multiple NOTCH targets, including *HEY1* and *HES1* (Figures 4H and S4C). Chromatin immunoprecipitation (ChIP) for STAT1 demonstrated that activation of antiviral signaling by CM or by coculture increased STAT1 occupancy in the *HEY1* promoter, particularly between the transcriptional start site (TSS) and −2kb where the ENCODE data were the most significant (Figure 4H). STAT1 ChIP analysis for *HES1* was similar (Figure S4C). Despite high constitutive NICD3, knockdown of STAT1 in 1833 IRDS-R decreased primary transcript and mRNA levels for *HES1* and *HEY1* after activation of antiviral signaling, which is consistent with the functional importance of at least some of the STAT1 sites in cooperating with NICD3 (Figure 4I). In contrast, although *NOTCH3* itself is a NOTCH target (Table S4), the proximal promoter of *NOTCH3* appears devoid of STAT1 sites by ENCODE. Accordingly, CM had no effect on the *NOTCH3* primary transcript (Figure S4D), suggesting that STAT1 affects transcription of NOTCH targets, rather than the *NOTCH3* gene. Thus, paracrine-activated STAT1 can cooperate with juxtacrine-activated NOTCH3 to augment the transcriptional response of multiple NOTCH targets.

STAT1 and NOTCH3 Control Stroma-Mediated Resistance through the Expansion of Therapy-Resistant Breast Cancer Cells

Both antiviral and NOTCH signaling have roles in controlling normal and cancer stem cells (Baldridge et al., 2010; Ranganathan et al., 2011). Indeed, NOTCH and its target genes were previously shown to help maintain a subpopulation of $CD44^{+}CD24^{low+}$ cells that have tumor-initiating properties (e.g., increased mammosphere and tumor formation) (Azzam et al., 2013). Because tumor-initiating cells (TICs) are known to be resistant to RT/chemo, we investigated whether stromal cell interaction might lead to the expansion of such therapy-resistant cells (TRCs). Indeed, coculture resulted in the upregulation of a gene signature associated with TICs (Shipitsin et al., 2007) (Figure 5A) and in the expansion of the $CD44^{+}CD24^{low+}$ subpopulation of 1833 IRDS-R (Figure 5B). This $CD44^{+}CD24^{low+}$ population is resistant to both RT and chemotherapy compared to $CD44^{+}CD24^{neg}$ counterparts (Figure 5C) and enriches after genotoxic damage (Figure S5A). Coculture with fibroblasts prior to seeding increased mammosphere formation (Figure 5D), and knockdown of STAT1 or inhibition of NOTCH3 with either RNAi or GSI inhibited both mammosphere formation (Figure 5E) and enhancement of the TIC gene signature (Figure 5A). Similar STAT1-dependent stromal cell activation of NOTCH3 and expansion of mammospheres were observed in other IRDS-Rs as well (Figures S5B–S5D). Constitutive activation of NOTCH3 in monoculture also led to modest expansion of both mammospheres and $CD44^{+}CD24^{low+}$ cells (Figures 5F and S5E). In accordance with an expansion of $CD44^{+}CD24^{low+}$ TRCs, the proportion of surviving mammospheres was higher after irradiation of cells seeded from coculture compared to monoculture (Figure 5G). Thus, these results suggest that STAT1 and NOTCH3 can drive expansion of breast cancer TRCs.

Like with STAT1, knockdown of NOTCH3 with multiple different siRNAs inhibited both stroma-mediated expansion of breast cancer TRCs and resistance (Figures 5H, S5F, and S5G). Inhibiting JAG1 also inhibited RT resistance after coculture with the greatest effect occurring after disruption in both 1833 IRDS-R and fibroblasts (Figures 5I and S5H), which is consistent with the interactome results showing JAG1 upregulation in both cell types. Expression of NICD3 in monoculture 1833 IRDS-R partially recapitulated the protective effect of stromal cells (Figure 5J). Similarly, ectopic NICD3 partially rescued

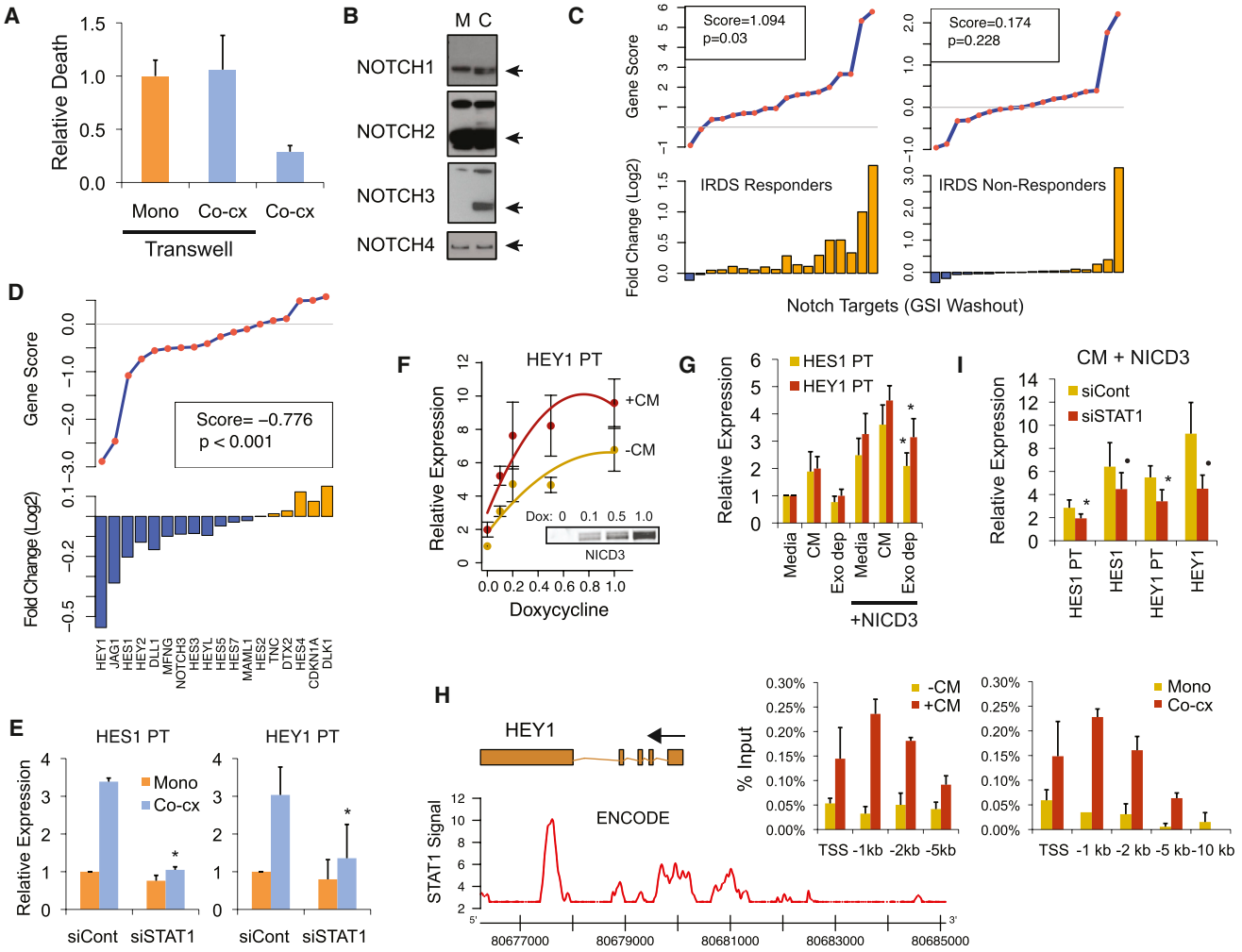

Figure 4. STAT1 Enhances the Transcriptional Response to Juxtacrine NOTCH3 Signaling that Is Required for Stroma-Mediated Protection

(A) Cell death of 1833 IRDS-R in coculture after RT. MRC5 fibroblasts were separated by a transwell filter large enough to allow exosome passage (n = 3).

(B) Immunoblot of the indicated NOTCH family members in 1833 IRDS-R after monoculture (M) or coculture (C). Arrow indicates cleaved intracellular domain.

(C and D) (C) Expression of NOTCH target genes in IRDS-R and IRDS-NR after coculture and (D) after STAT1 knockdown in 1833 IRDS-R after coculture. NOTCH targets were experimentally defined by GSI washout (Table S4) and were used in Gene Set Analysis.

(E) Expression of the indicated NOTCH target gene primary transcript (PT) in 1833 IRDS-R (n = 3).

(F) Expression of *HEY1* PT in response to doxycycline (Dox)-induced NICD3 in 1833 IRDS-R with or without addition of coculture CM (mean ± SEM, n = 6–8). Inset shows NICD3 levels after Dox addition (μg/ml).

(G) Expression of the indicated primary transcripts to NICD3 after addition of coculture CM or CM depleted of exosomes (Exo dep). CM compared to CM depleted of exosomes is used for significance levels (mean ± SEM, n = 4–6).

(H) ENCODE ChIP data for STAT1 occupancy of the *HEY1* proximal promoter region is shown along the indicated genomic coordinates. Bar plots show STAT1 ChIP from 1833 IRDS-R with and without addition of CM (left) and after mono- or coculture (right). Relative position upstream of the TSS is labeled on the x axis for each bar plot. Shown are two representative experiments (mean ± SD) out of four total.

(I) Expression of *HEY1* and *HES1* mRNA or primary transcripts in response to NICD3 and coculture CM in 1833 IRDS-R with and without STAT1 knockdown (mean ± SEM, n = 4–7). ●$p < 0.10$ and *$p < 0.05$.

Unless noted, all bar plots in figure are mean ± SD of *n* biological replicates. See also Figure S4.

the effect of STAT1 knockdown on stromal cell protection (Figure 5K). These partial effects on resistance parallel the partial transcriptional responses of NOTCH target genes when only STAT1 or NOTCH3 were fully engaged. Together, these data suggest that stroma-mediated resistance results from cooperation between STAT1 and NOTCH3 to expand and/or maintain breast cancer TRCs.

NOTCH Inhibition Reverses Stroma-Mediated Resistance of IRDS Responders and Improves Survival In Vivo

Considering that the NOTCH3 and STAT1 pathways are necessary for stroma-mediated resistance in IRDS-Rs, we investigated whether a GSI could selectivity reverse the protective effects of stromal cells. For IRDS-Rs, treatment with the GSI

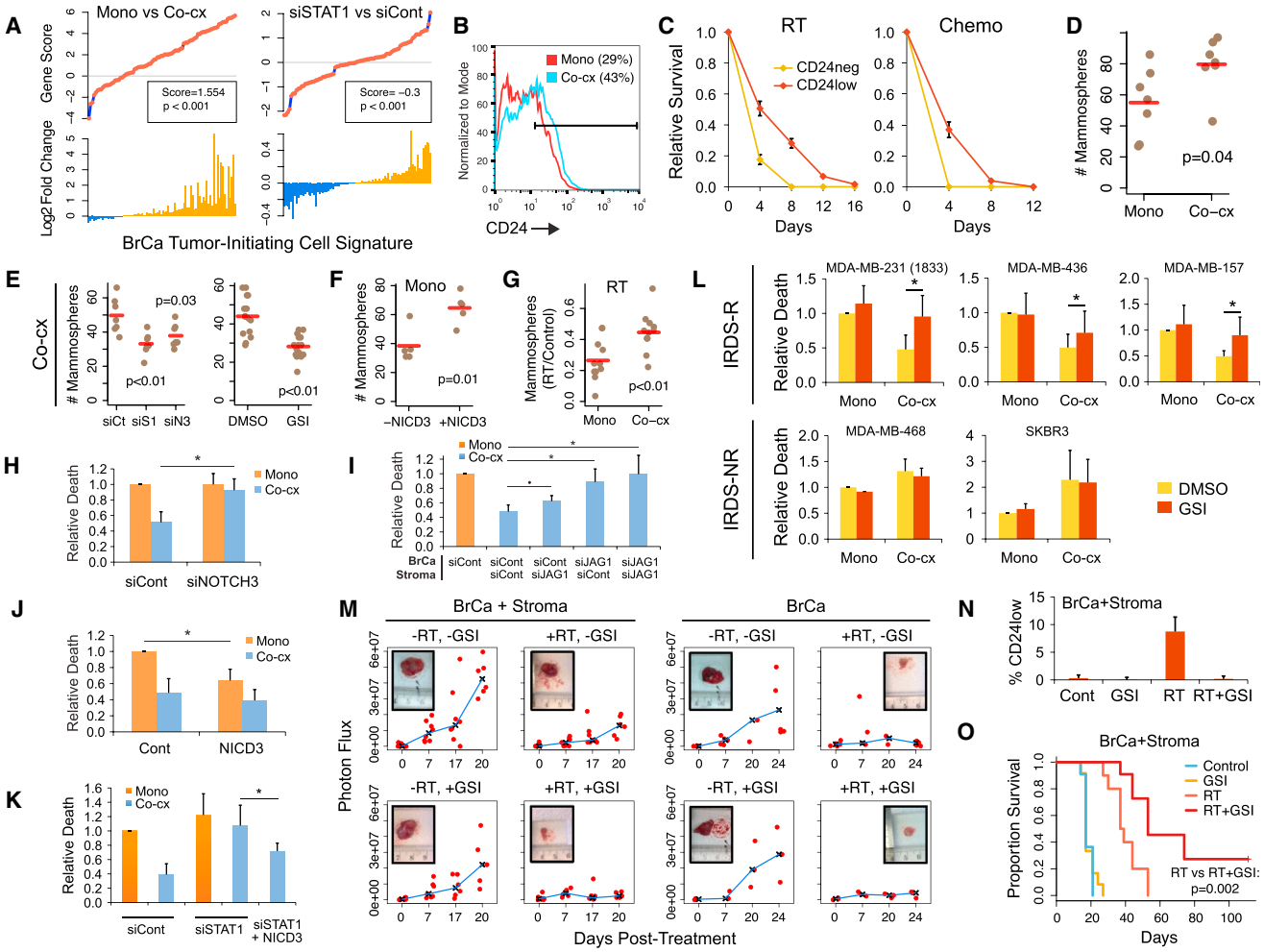

Figure 5. Stromal Cells Drive the Expansion of a Subpopulation of Therapy-Resistant Breast Cancer Cells through Antiviral STAT1 and NOTCH3 Signaling

(A) Gene Set Analysis comparing IRDS-R in monoculture versus coculture with MRC5 fibroblasts or comparing 1833 IRDS-R in coculture transfected with siSTAT1 versus siControl.

(B) Percentage of $CD44^{+}CD24^{low+}$ 1833 IRDS-R after coculture with MRC5. All $CD24^{low+}$ cells are also $CD44^{+}$.

(C–E) (C) Survival of sorted $CD44^{+}CD24^{low+}$ and $CD44^{+}CD24^{neg}$ cells after 10 Gy RT or 4 μM doxorubicin (chemo). Number of mammospheres from 1833 IRDS-R after (D) coculture or (E) coculture following knockdown of STAT1 (siS1), NOTCH3 (siN3), or control (siCt) or after treatment with the GSI DAPT.

(F) Number of mammospheres after NICD3 induction by doxycycline in monoculture.

(G–K) (G) Proportion of surviving mammospheres relative to untreated control in mono- or coculture after 3 Gy RT. Cell death after 10 Gy RT following (H) knockdown of NOTCH3 in 1833 IRDS-R, (I) knockdown of JAG1 in 1833 IRDS-R, MRC5 (Stroma), or both (n = 4); (J) expression of NICD3 (n = 7); or (K) STAT1 knockdown with and without NICD3 expression (n = 3–4).

(L) Cell death of IRDS-Rs and IRDS-NRs after 10 Gy RT and treatment with the GSI DAPT or DMSO (n = 5–10).

(M) Photon flux from mice xenografted subcutaneously with luciferase-labeled 1833 IRDS-R with or without MRC5 fibroblasts (Stroma) and treated 7 days later with 8 Gy RT, the GSI DAPT, both, or untreated. Mean values (black "X") are connected by blue line. Representative tumors after treatment are inset. In presence of stroma, tumor response was associated with RT ($p < 0.001$) and GSI ($p = 0.004$). Without stroma, RT ($p = 0.019$), but not GSI ($p = 0.79$), was associated with response.

(N) Percentage of $CD44^{+}CD24^{low+}$ cells in tumors from mice xenografted with 1833 IRDS-R with and without MRC5 stroma 7 days after the indicated treatment.

(O) Survival of these mice, which are independent cohorts from that used in Figure 5M. *$p < 0.05$.

Unless noted, all bar plots in figure are mean ± SD of *n* biological replicates. See also Figure S5.

DAPT completely or partially reversed the protective effects of fibroblasts and had only small effects in monoculture (Figure 5L). In contrast, for IRDS-NRs, neither coculture nor GSI discernibly affected cytotoxicity after RT. In vivo, admixing fibroblasts with luciferase-labeled 1833 IRDS-R resulted in the upregulation of NOTCH targets (Figure S5I). Treatment with GSI alone decreased NOTCH targets (Figure S5J) but had only a mild or insignificant effect on breast cancer growth in the presence ($p = 0.083$) or absence ($p = 0.67$) of admixed fibroblasts (Figure 5M). With RT, the presence of fibroblasts protected breast

cancer ($p = 0.026$); however, three consecutive doses of GSI starting from the day of RT reversed this protection. Moreover, GSI prevented the in vivo enrichment of $CD44^{+}CD24^{low+}$ TRCs observed after RT (Figure 5N), and the combination of RT and GSI rendered nearly 30% of mice tumor free, as compared to 0% with RT or GSI alone (Figure 5O). Thus, for IRDS-R basal-like breast cancers, the combination of GSI and genotoxic therapy prevents stroma-mediated expansion of TRCs adept at tumor reinitiation.

Expression of Antiviral and NOTCH3 Pathways in Primary Human and Mouse Basal-like Breast Cancer

To investigate potential disease relevance, we examined whether basal subtype primary human breast cancers show expression and activation of antiviral/NOTCH3 pathways in ways predicted by our experimental models. We first analyzed protein expression of RAB27B, STAT1, and NOTCH3 in primary human triple-negative breast cancers (TNBC), which overlap with the basal subtype. RAB27B showed strong stromal staining in 71% of TNBC tumors (Figure 6A). By image analysis, the intensity of STAT1 preferentially exhibited a strong tumor-stroma border pattern also in 71% of TNBC samples. For NOTCH3, this tumor-stroma border pattern was more subtle, possibly because NOTCH3 and JAG1 are themselves NOTCH targets, but was discernible in 29% of TNBC cases. Examination of tumors from TNBC patient-derived xenografts (PDX) also demonstrated strong tumor-stroma border patterns for STAT1 and NOTCH3 (Figure 6B). Moreover, breast tumors from the $K14cre;BRCA1^{F/F};p53^{F/F}$ mice, which are a model of basal subtype breast cancer (Liu et al., 2007), revealed patterns of staining similar to primary human TNBC (Figure 6B). In contrast, a distinct tumor-stroma border pattern was rarely observed in ER+ primary tumors for either STAT1 (14%) or NOTCH3 (0%) and was not observed in ER+ PDX tumors (Figure S6A). Thus, in both human and mouse basal-like tumors, key drivers of anti-viral/NOTCH3 signaling can show preferential localization around sites of tumor-stroma interaction.

To investigate whether similarities in localization of antiviral and NOTCH3 proteins between in vivo tumors and in vitro models are accompanied by expected gene expression changes in IRDS and NOTCH target genes, we used three distinct sets of gene expression data from primary human breast cancer. The Stroma series is a 53-sample set of breast cancer stroma and adjacent normal stroma, the NKI295 series is composed of 295 primary human breast tumors confirmed to be largely cancer cells, and the LCMD series contains 28 paired primary tumor and stroma samples that were separated by laser-capture microdissection. Consistent with breast cancer inducing stromal RAB27B, the Stroma series revealed higher *RAB27B* expression in tumor stroma compared to adjacent normal, whereas other RABs on average had similar or decreased expression (Figure 6C). Using the NKI295 series, *RIG-I* was the best predictor of IRDS status compared to other PRRs and interferon-related genes (Figure 6D). Of all available NOTCH family receptors and ligands on the LCMD series array (Figure 6E), breast cancer *NOTCH3* and stromal *JAG1* were the best at predicting expression of breast cancer NOTCH targets (Table S4) as measured by their average expression (metagene). Moreover, when breast cancer *NOTCH3* was paired with breast cancer *RIG-I*, and stromal *JAG1* was paired with stromal *RAB27B*, high expression of the two pairs cooperatively predicted high NOTCH metagene expression (Figures S6B and S6C). In total, these data indicate that gene expression changes attributed to the antiviral and NOTCH3 pathways can be observed in primary tumors.

Because STAT1 enhances the transcriptional response to NOTCH3 in IRDS-R breast cancer, high NOTCH target gene expression is expected to associate with high NOTCH3/JAG1 and high STAT1 activity in basal subtype tumors. To examine this, we used the NKI295 series and substituted stromal *JAG1* with breast cancer *JAG1*, as stromal genes cannot be evaluated and breast cancer *JAG1* was comparable to stromal *JAG1* at predicting NOTCH target gene expression (Figure S6D). For STAT1 activity, we used the clinical IRDS classifier because it includes *STAT1*, and STAT1 both regulates (Figure 1H) and correlates with IRDS status (Spearman's correlation coefficient 0.79, $p < 0.001$). As expected, increasing *NOTCH3* resulted in higher likelihood of NOTCH pathway activation (Figure 7A). The probability was highest when *NOTCH3*, *JAG1*, and IRDS were all high, particularly for basal subtype tumors (red dots, top right plot), a result that was recapitulated in basal-like tumors from the $K14cre;BRCA1^{F/F};p53^{F/F}$ mouse model (Figure 7B). Thus, these results suggest that antiviral signaling preferentially facilitates the transcriptional response to NOTCH3 in primary human and mouse basal subtype tumors.

Antiviral/NOTCH3 Pathway Genes Predict Clinical Resistance to Chemotherapy and RT

Having shown that *NOTCH3* and the IRDS contribute to predicting NOTCH activation in the NKI295 series, we examined whether both pathways function together to predict clinical resistance to chemotherapy and RT. *NOTCH3* was dichotomized using a mean cut-point, and for consistency, IRDS status was defined using our original seven gene clinical classifier. Interestingly, 31% of *NOTCH3*(hi)/IRDS(+) tumors belonged to either the basal or claudin-low subtype (Figure 7C; $p < 0.01$ by chi-square test), two basal-like subtypes that are enriched in cancer stem-cell-like features (Prat et al., 2010). Consistent with this, *NOTCH3*(hi)/IRDS(+) tumors showed enrichment of the same breast cancer TIC signature upregulated in IRDS-R cells after coculture (Figures 7C and 5A), suggesting that these tumors could also contain TRCs. Indeed, among the patients who received chemotherapy, those with the highest risk of breast-cancer-specific death were *NOTCH3*(hi)/IRDS(+) (Figure 7D). Cox regression using continuous values rather than arbitrary cut-offs for *NOTCH3* demonstrated that higher *NOTCH3* augmented risk only among patients with tumors that were IRDS(+) and/or basal subtype (Figure 7E). The effect of both pathways on survival was distinct from metastasis risk as both were independent of the MammaPrint metastasis signature (van de Vijver et al., 2002), and neither were predictive among patients not receiving chemotherapy (Figure S7A). *NOTCH3* (hi)/IRDS(+) patients were also the most likely to fail RT (Figure 7F). Finally, using the Stroma series, we found that high stromal *RAB27B* predicted poor survival, whereas other RABs

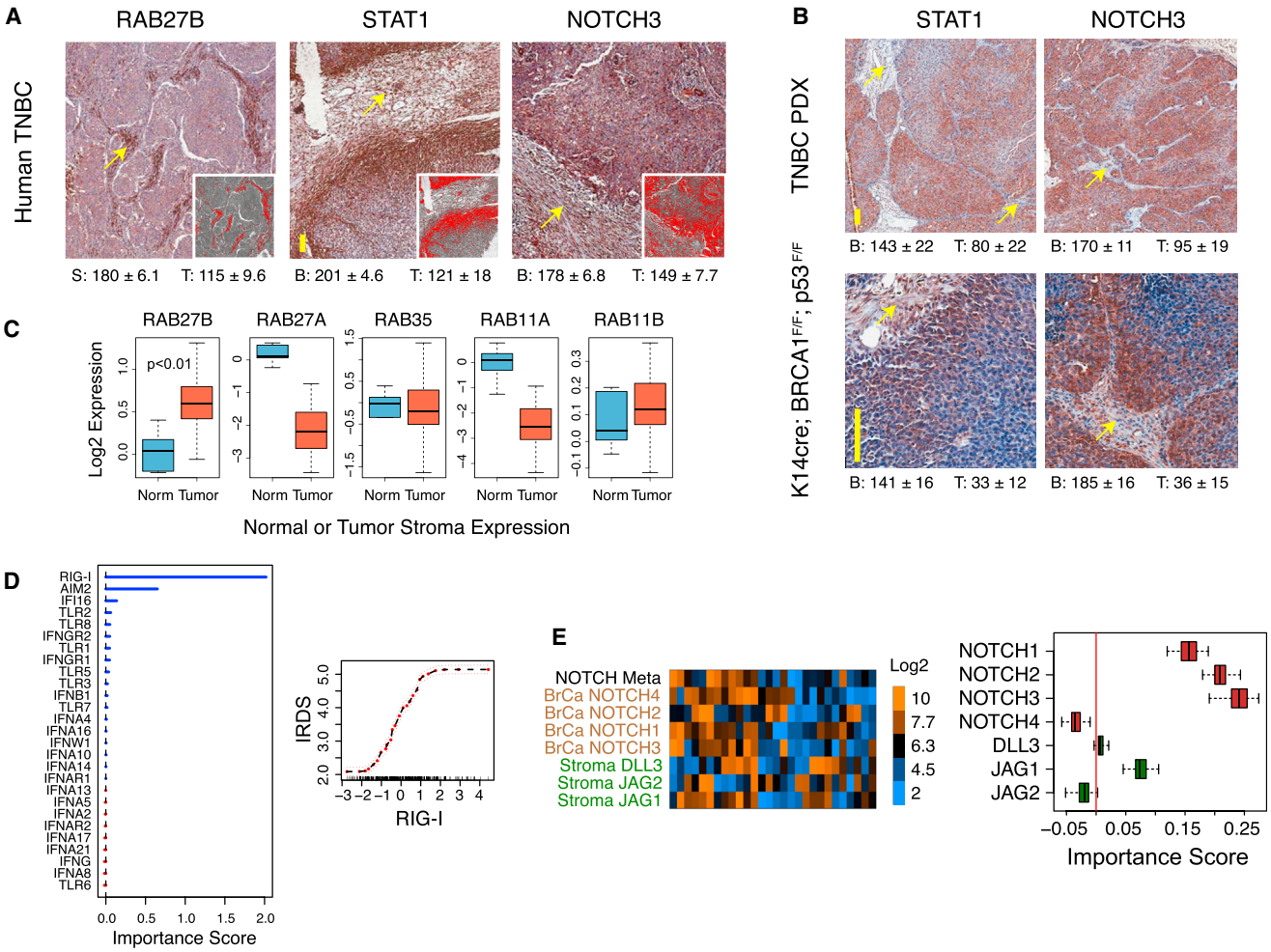

Figure 6. Expression of Antiviral and NOTCH3 Pathway Predicts IRDS and NOTCH Target Gene Expression in Primary Human and Mouse Tumors

(A and B) (A) Expression of RAB27B, STAT1, and NOTCH3 in primary human triple-negative breast cancer (TNBC) or (B) in TNBC patient-derived xenografts (PDX) and basal-like tumors from K14Cre;BRCA1$^{F/F}$;p53$^{F/F}$ conditional knockout mice. Arrows show representative areas of stroma. Insets for TNBC images show darker staining regions (red) segmented from lighter regions. Semiquantitation of expression in stroma (S), tumor (T), or tumor-stroma borders (B) is indicated. Vertical bar is 200 microns. A total of seven primary TNBC tumors were scored. Two out of two PDX and three out of three mouse tumors gave similar results. Shown are representative images and semiquantitation.

(C) Box-and-whisker plots of expression values for the indicated RABs from primary human breast cancer stroma (Tumor) or normal stroma (Norm) using the stroma series.

(D) Importance scores (higher is more predictive) from a RF regression model (variance explained: 55.1%) to predict breast cancer IRDS expression using the NKI295 series. Adjusted effect of *RIG-I* on IRDS expression (right).

(E) Heat map and scale showing expression of all available NOTCH receptors in breast cancer (brown) and NOTCH ligands in stroma (green) from the LCMD series. These were used to predict the average expression of NOTCH target genes in breast cancer (variance explained: 30.2% ± 1.1%) defined by GSI washout (NOTCH Meta). On the right are importance scores from Monte Carlo replications.

See also Figure S6.

showed no association (Figures 7G and S7B). In total, the antiviral/NOTCH3 pathways predict clinical resistance, particularly for basal subtype tumors.

DISCUSSION

We demonstrate that interaction of stromal cells with breast cancer cells results in paracrine and juxtacrine signaling events to drive stroma-mediated resistance (Figure 7H). First, stromal cells increase RAB27B and transfer 5′-triphosphate RNA in exosomes to activate RIG-I antiviral signaling in breast cancer cells. Second, breast cancer cells induce NOTCH3 to make the receptor available for engagement with JAG1. The paracrine and juxtacrine pathways converge as STAT1 facilitates the transcriptional response to NOTCH3, resulting in the expansion of therapy-resistant TICs. Consistent with this, stromal cells mediate both decreased cell death and continued tumor growth after RT. Blocking the NOTCH pathway resensitizes

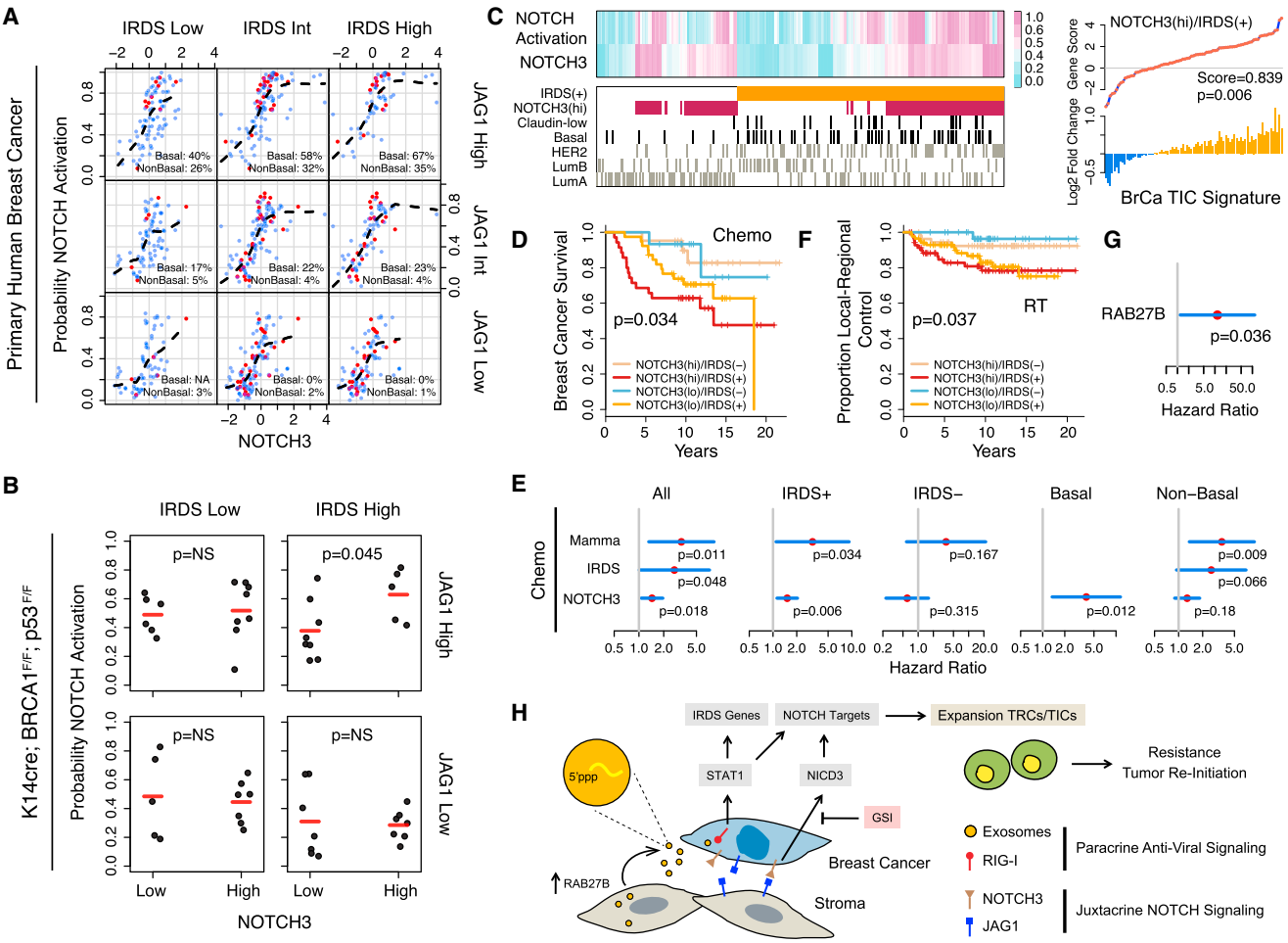

Figure 7. NOTCH3 and STAT1/IRDS Cooperate to Predict NOTCH Target Genes and Clinical Resistance to Chemotherapy and RT Preferentially in Basal-like Breast Cancers

(A and B) Prediction of NOTCH target gene expression by IRDS and *NOTCH3*/*JAG1* in (A) primary human tumors and in (B) basal-like tumors from the K14Cre;BRCA1$^{F/F}$;p53$^{F/F}$ conditional knockout mice. For human tumor analysis, the NKI295 series was used. The probability of NOTCH pathway activation as measured by the NOTCH metagene is shown on the y axis with probabilities for basal (red dots) or nonbasal (blue dots) tumors displayed separately. The percentage of tumors with greater than 80% probability of NOTCH activation is inset. A LOWESS regression line (black dashed line) is shown. IRDS and *JAG1* were equally divided into low, intermediate, and high values. For mouse tumor analysis, IRDS, *NOTCH3*, and *JAG1* expression were dichotomized into only high and low due to smaller sample size. Mean value is marked by red line.

(C) Heat map showing probabilities of NOTCH activation and *NOTCH3* expression for each patient (columns) in the NKI295 series. All values are scaled between 0 and 1. Hatches below the heat map show status for IRDS(+), *NOTCH3*(hi), and the indicated molecular subtypes. On the right is Gene Set Analysis for the same TIC signature used in Figure 5A and compares *NOTCH3*(hi)/IRDS(+) tumors to those that are *NOTCH3*(lo) and/or IRDS(−).

(D) Survival after adjuvant chemotherapy of patients from the NKI295 series stratified by *NOTCH3* and IRDS. Overall p value is shown.

(E) Hazard ratios and 95% confidence intervals from Cox regression analysis for breast cancer survival using *NOTCH3* as a continuous variable, IRDS status (positive versus negative), and MammaPrint (Mamma) metastasis signature status (positive versus negative). All patients received adjuvant chemotherapy. Hazard ratio for *NOTCH3* is per unit increase in expression. Analyses are also stratified by IRDS status and basal versus nonbasal subtype tumors. Values are not shown if there are too few patients in the group.

(F) Relapse in irradiated region (local-regional control) after adjuvant RT.

(G) Hazard ratio from Cox regression for relapse in the Stroma series using stromal *RAB27B* as a continuous variable.

(H) Model of the tumor-stroma antiviral/NOTH3 pathways controlling RT/chemo resistance.

See also Figure S7.

tumors to RT, rendering mice tumor free. These biological interactions between antiviral and NOTCH3 signaling are mirrored by statistical evidence that they jointly influence NOTCH activation and treatment resistance in primary human basal-like breast cancers.

The role of exosomes in cancer as mediators of cell-cell communication with the microenvironment has gained increasing attention. Functionally, exosomes have intriguing and elaborate roles in cancer progression and can transfer a variety of proteins, DNA, and RNA that can explain some of their effects

(Peinado et al., 2012; Valadi et al., 2007). Our data suggest that RNA contained within exosomes is enriched in noncoding transcripts and can activate RIG-I. Consistent with the known properties of RIG-I stimulatory viral RNA (Loo and Gale, 2011), 5′-triphosphate is similarly required for exoRNA to activate RIG-I. Sequencing exoRNA revealed no evidence of viral transcripts—rather, exoRNA was enriched in transposable elements and other repetitive sequences, many of which are known or putative RNA polymerase III transcripts. RNA polymerase III transcripts can contain 5′-triphosphate and likely are largely noncoding (Dieci et al., 2013). Although the quantity and diversity of noncoding human transcripts is large (ENCODE Project Consortium, 2012) and RIG-I is not known to overtly show sequence-specific binding, the enrichment for transposable elements and other repetitive elements in exosomes is interesting given the viral origins of some of these sequences (Belancio et al., 2010). Despite prolific incorporation into the genome, it is notable that these elements are normally transcriptionally silenced but can be derepressed to high levels in cancer (Ting et al., 2011). When expressed, these elements can also exhibit subcellular partitioning into the nucleus and the cytoplasm (Goodier et al., 2010). Accumulation of transposable elements can result in autoimmunity with elevated ISGs in normal tissue (Stetson et al., 2008). Thus, our results suggest that noncoding RNA found in exosomes and similar microvesicles (Balaj et al., 2011; Li et al., 2013a) may coax antiviral responses to influence treatment resistance, potentially adding to the increasing evidence that atypical RNA transcripts can contribute to human disease.

Both antiviral/interferon signaling and the NOTCH pathway are known to regulate the maintenance of normal and cancer stem-like cells. Interestingly, inflammatory/stress signaling involving STAT can function with NOTCH signaling in development and in homeostasis to influence self-renewal (Kux and Pitsouli, 2014). For example, in *Drosophila*, inflammation and stress in the midgut leads to compensatory intestinal stem cell proliferation that is regulated by STAT. STAT can be activated non-cell-autonomously by damaged cells, while distinct levels of NOTCH control intestinal stem cell commitment and differentiation. Our findings that stromal fibroblasts can secrete exosomes to induce antiviral signaling in breast cancer cells and that STAT1 promotes NOTCH3-driven expansion of therapy resistant TICs highlight an unexpected way that these two evolutionarily conserved pathways converge to influence cell fate in cancer.

The mechanisms whereby basal-like tumors are preferentially protected by stroma through antiviral/NOTCH3 signaling require further investigation. One mechanism indicated herein may be the capacity of basal-like breast cancer cells to coerce stromal cells to augment exosome secretion. RAB27B is uniquely induced in stromal cells by IRDS-R but not IRDS-NR breast cancer, and evidence from primary human tumors also distinguishes it from other RABs. However, alternative methods to either increase exosome production in the microenvironment or instigate similar antiviral signaling (e.g., immune cells) may also exist. Other factors that might contribute to differences in the way basal-like tumors respond to stroma include defects in the BRCA1 pathway, which have been associated with basal and claudin-low tumors (Prat et al., 2010). It is notable that two of the IRDS-R breast cancer cell lines have reported mutations in BRCA1 (Elstrodt et al., 2006), and BRCA1 null mouse mammary tumors show evidence for the antiviral/NOTCH3 pathway. As a cell extrinsic mechanism of resistance, the protective effect of stroma may be critical for certain breast cancers with intrinsic DNA damage sensitivity.

Extrapolating the relevance of findings from model systems to human disease is often challenging. In this study, extensive statistical modeling of primary tumor expression data was used to support the mechanisms dissected from experimental models. Specifically, primary tumor data suggest that (1) RIG-I is a driver of the IRDS, (2) breast cancer NOTCH3 and stromal JAG1 are important regulators of NOTCH target gene expression, (3) NOTCH3 and STAT1 are localized to sites of tumor-stroma interaction, (4) STAT1 facilitates the transcriptional response to NOTCH3, (5) IRDS/STAT1 and NOTCH3 identify patients with both high NOTCH target genes and chemo/RT resistant tumors, and (6) high IRDS/NOTCH3 is preferentially observed in basal and claudin-low subtype primary tumors, which are known to be enriched in cancer stem-cell-like features (Prat et al., 2010). These observations, combined with preclinical studies showing that GSI can reverse the effects of stromal cells on TRC expansion, tumor growth after genotoxic damage, and survival suggest the disease relevance of our findings. Together, the antiviral and NOTCH3 pathways may serve as companion biomarkers and druggable targets for stroma-mediated resistance.

EXPERIMENTAL PROCEDURES

Cell Culture and Cell Death Assays

Breast cancer and stromal cell lines used in this study are listed in Table S1. For cocultures, breast cancer cells were labeled with CFSE and mixed 1:1 with stromal cells, typically MRC5 fibroblasts unless otherwise noted. CM was harvested at 48 hr from subconfluent cultures and added directly for 24–48 hr. CM from monoculture was used as a control. For cell death assays, mono- or cocultures were irradiated at 48 hr with 10 Gy. Cell death of CFSE-labeled breast cancer cells was measured at 96 hr post-RT by flow cytometry using Sytox-Red. For GSI treatment, 10 μM DAPT or DMSO control was used.

Exosome Isolation and Analysis

Cells were grown in exosome-depleted media, and exosomes were isolated from CM collected at 48 hr by serial centrifugation. For exosome assays, an equal volume of exosomes was added to cells for 24–48 hr. For exosome depletion, CM was ultracentrifuged overnight. Dye transfer was visualized by microscopy or by flow cytometry at 24 hr. ExoRNA was extracted after 48 hr of culture using TRIzol. Assays were performed at 16–24 hr after transfection of 10–100 ng exoRNA using RNAiMax.

Chromatin Immunoprecipitation and Primary Transcript Analysis

Breast cancer cells were cocultured with MRC5 fibroblasts or treated with CM for 48 hr. NICD3 was induced with 0.1 μg/ml doxycycline for 72 hr.

Mammosphere Analysis

CFSE-labeled breast cancer cells cultured with or without MRC5 fibroblasts were sorted by FACS. siRNA knockdown was performed 1 day before coculture, and doxycycline was added for 1 week to induce NICD3. Cells were seeded at 10,000 per well. After 7 days, spheres larger than 100 μm were counted.

In Vivo Mouse Studies

1×10^6 MDA-MB-231 1833 cells with and without an equal number of MRC5 fibroblasts were injected with Matrigel into the flanks of 6- to 8-week-old female nude mice. Starting at day 7, tumors were irradiated with 8 Gy, and mice were treated with three daily doses of DAPT at 10 mg/kg.

Statistical Analysis and Computational Modeling

Unless otherwise noted, results reported are mean ± SD of *n* independent biological replicates. For comparisons of the mean between two groups, a two-tailed two-sample t test was employed. Genes upregulated from transcriptomic analysis of tumor-stromal cell interaction are listed in Tables S2, S3, and S5. NOTCH targets and IRDS genes used in computational studies are listed in Tables S4 and S6.

ACCESSION NUMBERS

The GEO accession number for the expression and sequencing data reported in this paper is GSE60998.

SUPPLEMENTAL INFORMATION

Supplemental Information includes Extended Experimental Procedures, seven figures, and six tables and can be found with this article online at http://dx.doi.org/10.1016/j.cell.2014.09.051.

AUTHOR CONTRIBUTIONS

M.C.B., T.J.W., and B.Y.N. contributed equally as co-first authors, and their names were ordered arbitrarily. M.C.B. and T.J.W. performed in vitro characterization of the stromal effect, defining the role for STAT1, NOTCH3, and therapy-resistant subpopulations. T.J.W. characterized the NOTCH pathway. B.Y.N. performed exosome and RIG-I studies. T.J.W. and B.Y.N. performed xenograft experiments. T.J.W., B.Y.N., and B.X. performed mammosphere studies. M.C.B. performed protein analysis of human and mouse tumors. B.X. performed STAT1 and NOTCH3 transcriptional studies. Y.Q. performed and analyzed sequencing studies. D.J.A. and J.S. designed, performed, and interpreted studies on tumor-initiating cells. P.J.t.-B. and J.J. established PDX and spontaneous tumor models. A.J.M. and H.I. performed and interpreted computational modeling. A.J.M. designed, analyzed, and interpreted experiments and wrote the manuscript.

ACKNOWLEDGMENTS

M.C.B. was supported by a fellowship from the Dutch Cancer Society. A.J.M. is a Department of Defense Era of Hope Scholar (W81XWH-09-1-0339). Support for this work and for B.X. was also provided by the Basser Center for BRCA Research. B.Y.N. and T.J.W. were supported by grants from the Department of Defense (W81XWH-12-1-0180 and W81XWH-09-1-0339). A.J.M., T.Y., and Y.Q. were supported by a grant from the NIH/NCI (5R01CA172651). Additional support was provided to H.I. and A.J.M. from the NIH (5R01CA163739) and to C.T. from an NIH training grant and career development award (DK007066 and TR000139). We would like to thank Danielle Loughlin for insightful discussions.

Received: September 10, 2013
Revised: June 11, 2014
Accepted: September 3, 2014
Published: October 23, 2014

REFERENCES

Aster, J.C., and Blacklow, S.C. (2012). Targeting the Notch pathway: twists and turns on the road to rational therapeutics. J. Clin. Oncol. *30*, 2418–2420.

Azzam, D.J., Zhao, D., Sun, J., Minn, A.J., Ranganathan, P., Drews-Elger, K., Han, X., Picon-Ruiz, M., Gilbert, C.A., Wander, S.A., et al. (2013). Triple negative breast cancer initiating cell subsets differ in functional and molecular characteristics and in γ-secretase inhibitor drug responses. EMBO Mol. Med. *5*, 1502–1522.

Balaj, L., Lessard, R., Dai, L., Cho, Y.-J., Pomeroy, S.L., Breakefield, X.O., and Skog, J. (2011). Tumour microvesicles contain retrotransposon elements and amplified oncogene sequences. Nat Commun. *2*, 180.

Baldridge, M.T., King, K.Y., Boles, N.C., Weksberg, D.C., and Goodell, M.A. (2010). Quiescent haematopoietic stem cells are activated by IFN-gamma in response to chronic infection. Nature *465*, 793–797.

Belancio, V.P., Roy-Engel, A.M., and Deininger, P.L. (2010). All y'all need to know 'bout retroelements in cancer. Semin. Cancer Biol. *20*, 200–210.

Buess, M., Nuyten, D.S.A., Hastie, T., Nielsen, T., Pesich, R., and Brown, P.O. (2007). Characterization of heterotypic interaction effects in vitro to deconvolute global gene expression profiles in cancer. Genome Biol. *8*, R191.

Chen, X., and Ishwaran, H. (2012). Random forests for genomic data analysis. Genomics *99*, 323–329.

Dieci, G., Conti, A., Pagano, A., and Carnevali, D. (2013). Identification of RNA polymerase III-transcribed genes in eukaryotic genomes. Biochim. Biophys. Acta *1829*, 296–305.

Dreux, M., Garaigorta, U., Boyd, B., Décembre, E., Chung, J., Whitten-Bauer, C., Wieland, S., and Chisari, F.V. (2012). Short-range exosomal transfer of viral RNA from infected cells to plasmacytoid dendritic cells triggers innate immunity. Cell Host Microbe *12*, 558–570.

Elstrodt, F., Hollestelle, A., Nagel, J.H.A., Gorin, M., Wasielewski, M., van den Ouweland, A., Merajver, S.D., Ethier, S.P., and Schutte, M. (2006). BRCA1 mutation analysis of 41 human breast cancer cell lines reveals three new deleterious mutants. Cancer Res. *66*, 41–45.

ENCODE Project Consortium (2012). An integrated encyclopedia of DNA elements in the human genome. Nature *489*, 57–74.

Fabbri, M., Paone, A., Calore, F., Galli, R., Gaudio, E., Santhanam, R., Lovat, F., Fadda, P., Mao, C., Nuovo, G.J., et al. (2012). MicroRNAs bind to Toll-like receptors to induce prometastatic inflammatory response. Proc. Natl. Acad. Sci. USA *109*, E2110–E2116.

Goodier, J.L., Mandal, P.K., Zhang, L., and Kazazian, H.H., Jr. (2010). Discrete subcellular partitioning of human retrotransposon RNAs despite a common mechanism of genome insertion. Hum. Mol. Genet. *19*, 1712–1725.

Kang, Y., Siegel, P.M., Shu, W., Drobnjak, M., Kakonen, S.M., Cordón-Cardo, C., Guise, T.A., and Massagué, J. (2003). A multigenic program mediating breast cancer metastasis to bone. Cancer Cell *3*, 537–549.

Khodarev, N.N., Beckett, M., Labay, E., Darga, T., Roizman, B., and Weichselbaum, R.R. (2004). STAT1 is overexpressed in tumors selected for radioresistance and confers protection from radiation in transduced sensitive cells. Proc. Natl. Acad. Sci. USA *101*, 1714–1719.

Korkaya, H., Liu, S., and Wicha, M.S. (2011). Breast cancer stem cells, cytokine networks, and the tumor microenvironment. J. Clin. Invest. *121*, 3804–3809.

Kux, K., and Pitsouli, C. (2014). Tissue communication in regenerative inflammatory signaling: lessons from the fly gut. Front. Cell Infect. Microbiol. *4*, 49.

Li, C.C., Eaton, S.A., Young, P.E., Lee, M., Shuttleworth, R., Humphreys, D.T., Grau, G.E., Combes, V., Bebawy, M., Gong, J., et al. (2013a). Glioma microvesicles carry selectively packaged coding and non-coding RNAs which alter gene expression in recipient cells. RNA Biol. *10*, 1333–1344.

Li, J., Liu, K., Liu, Y., Xu, Y., Zhang, F., Yang, H., Liu, J., Pan, T., Chen, J., Wu, M., et al. (2013b). Exosomes mediate the cell-to-cell transmission of IFN-α-induced antiviral activity. Nat. Immunol. *14*, 793–803.

Liu, X., Holstege, H., van der Gulden, H., Treur-Mulder, M., Zevenhoven, J., Velds, A., Kerkhoven, R.M., van Vliet, M.H., Wessels, L.F., Peterse, J.L., et al. (2007). Somatic loss of BRCA1 and p53 in mice induces mammary tumors with features of human BRCA1-mutated basal-like breast cancer. Proc. Natl. Acad. Sci. USA *104*, 12111–12116.

Loo, Y.-M., and Gale, M., Jr. (2011). Immune signaling by RIG-I-like receptors. Immunity *34*, 680–692.

Luga, V., Zhang, L., Viloria-Petit, A.M., Ogunjimi, A.A., Inanlou, M.R., Chiu, E., Buchanan, M., Hosein, A.N., Basik, M., and Wrana, J.L. (2012). Exosomes mediate stromal mobilization of autocrine Wnt-PCP signaling in breast cancer cell migration. Cell *151*, 1542–1556.

McAuliffe, S.M., Morgan, S.L., Wyant, G.A., Tran, L.T., Muto, K.W., Chen, Y.S., Chin, K.T., Partridge, J.C., Poole, B.B., Cheng, K.-H., et al. (2012). Targeting

Notch, a key pathway for ovarian cancer stem cells, sensitizes tumors to platinum therapy. Proc. Natl. Acad. Sci. USA *109*, E2939–E2948.

McMillin, D.W., Negri, J.M., and Mitsiades, C.S. (2013). The role of tumour-stromal interactions in modifying drug response: challenges and opportunities. Nat. Rev. Drug Discov. *12*, 217–228.

Peinado, H., Alečković, M., Lavotshkin, S., Matei, I., Costa-Silva, B., Moreno-Bueno, G., Hergueta-Redondo, M., Williams, C., García-Santos, G., Ghajar, C., et al. (2012). Melanoma exosomes educate bone marrow progenitor cells toward a pro-metastatic phenotype through MET. Nat. Med. *18*, 883–891.

Prat, A., Parker, J.S., Karginova, O., Fan, C., Livasy, C., Herschkowitz, J.I., He, X., and Perou, C.M. (2010). Phenotypic and molecular characterization of the claudin-low intrinsic subtype of breast cancer. Breast Cancer Res. *12*, R68.

Ranganathan, P., Weaver, K.L., and Capobianco, A.J. (2011). Notch signalling in solid tumours: a little bit of everything but not all the time. Nat. Rev. Cancer *11*, 338–351.

Raposo, G., and Stoorvogel, W. (2013). Extracellular vesicles: exosomes, microvesicles, and friends. J. Cell Biol. *200*, 373–383.

Shipitsin, M., Campbell, L.L., Argani, P., Weremowicz, S., Bloushtain-Qimron, N., Yao, J., Nikolskaya, T., Serebryiskaya, T., Beroukhim, R., Hu, M., et al. (2007). Molecular definition of breast tumor heterogeneity. Cancer Cell *11*, 259–273.

Stetson, D.B., Ko, J.S., Heidmann, T., and Medzhitov, R. (2008). Trex1 prevents cell-intrinsic initiation of autoimmunity. Cell *134*, 587–598.

Théry, C., Ostrowski, M., and Segura, E. (2009). Membrane vesicles as conveyors of immune responses. Nat. Rev. Immunol. *9*, 581–593.

Ting, D.T., Lipson, D., Paul, S., Brannigan, B.W., Akhavanfard, S., Coffman, E.J., Contino, G., Deshpande, V., Iafrate, A.J., Letovsky, S., et al. (2011). Aberrant overexpression of satellite repeats in pancreatic and other epithelial cancers. Science *331*, 593–596.

Valadi, H., Ekström, K., Bossios, A., Sjöstrand, M., Lee, J.J., and Lötvall, J.O. (2007). Exosome-mediated transfer of mRNAs and microRNAs is a novel mechanism of genetic exchange between cells. Nat. Cell Biol. *9*, 654–659.

van de Vijver, M.J., He, Y.D., van't Veer, L.J., Dai, H., Hart, A.A., Voskuil, D.W., Schreiber, G.J., Peterse, J.L., Roberts, C., Marton, M.J., et al. (2002). A gene-expression signature as a predictor of survival in breast cancer. N. Engl. J. Med. *347*, 1999–2009.

Weichselbaum, R.R., Ishwaran, H., Yoon, T., Nuyten, D.S.A., Baker, S.W., Khodarev, N., Su, A.W., Shaikh, A.Y., Roach, P., Kreike, B., et al. (2008). An interferon-related gene signature for DNA damage resistance is a predictive marker for chemotherapy and radiation for breast cancer. Proc. Natl. Acad. Sci. USA *105*, 18490–18495.